THE JOURNAL OF PHYSICAL CHEMISTRY B

Article

pubs.acs.org/JPCB

Molecular Mechanism of Myoglobin Autoxidation: Insights from Computer Simulations

J. P. Arcon,[†,‡,§] P. Rosi,[†,§] A. A. Petruk,[†] M. A. Marti,*[,†,‡] and D. A. Estrin*[,†]

[†]Departamento de Química Inorgánica, Analítica y Química Física e INQUIMAE-CONICET, Facultad de Ciencias Exactas y Naturales, Universidad de Buenos Aires, Ciudad Universitaria, Pabellón 2, C1428EHA, Ciudad de Buenos Aires, Argentina

[‡]Departamento de Química Biológica, Facultad de Ciencias Exactas y Naturales, Universidad de Buenos Aires, Ciudad Universitaria, Pabellón 2, C1428EHA, Ciudad de Buenos Aires, Argentina

Supporting Information

ABSTRACT: Myoglobin (Mb) and hemoglobin have the biological ability to carry/store oxygen (O_2), a property which requires its heme iron atom to be in the ferrous -Fe(II)- state. However, the thermodynamically stable state in the presence of O_2 is Fe(III) and thus the oxidation rate of a globin is a critical parameter related to its function. Mb has been extensively studied and many mutants have been characterized regarding its oxygen mediated oxidation (i.e., autoxidation) rates. Site directed mutants in residues 29 (B10), which shapes the distal cavity, and 64 (E7), the well-known histidine gate, have been shown to display a wide range of autoxidation rate constants. In this work, we have thoroughly studied the mechanism underlying the autoxidation process by means of state-of-the-art computer simulation methodologies, using Mb and site directed mutants as benchmark cases. Our results explain the observed autoxidation rate tendencies in different variants of Mb, L29F < wt < L29A = H64Q < H64F < H64A, and shed light on several aspects of the reaction at the atomic level. First, water access to the distal pocket is a key event and the observed acid catalysis relies on HisE7 protonation and opening of the His gate to allow water access, rather than protonation of the oxy heme itself. Our results also suggest that the basic mechanism, i.e., superoxide displacement by hydroxide anion, is energetically more feasible. Finally, we confirmed that distal hydrogen bonds protect the oxy complex from autoxidation.

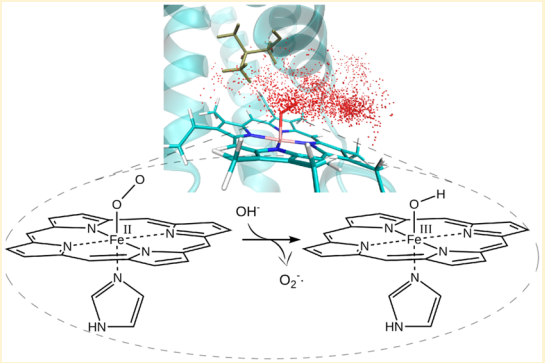

INTRODUCTION

In mammals, myoglobin (Mb) has an important physiological role in skeletal muscle and heart muscle cells which is to store and transport oxygen (O_2) from the sarcolemma to the mitochondrion allowing efficient work of the respiratory electron transfer chain.[1] The oxidation state of the heme iron is crucial for this function since oxygen only binds to the ferrous heme −Fe(II)−. Interestingly, for most if not all heme proteins the thermodynamically stable state is the ferric heme −Fe(III)−. Thereby, in the presence of oxygen (i.e., air) heme proteins, including Mb, become oxidized in a process known as autoxidation. This reaction occurs spontaneously in physiological conditions and cells rereduce Mb, as well as hemoglobin, actively.[2,3] Similar behavior is observed in many heme proteins, especially globins from numerous organisms, which require a ferrous heme to fulfill their task. Thus, avoiding heme autoxidation is critical for their normal function. In addition, Mb autoxidation has been recently reported to play a key role in myocardial ischemia reperfusion.[4]

Physiologically, the autoxidation process is kinetically controlled. First kinetic measurements showed that under low oxygen pressure the autoxidation rate is first order in oxygen concentration/pressure. However, it becomes independent of oxygen concentration at p_{O_2} values around p_{50} (which is the oxygen pressure required to half load the protein with it), strongly suggesting that autoxidation requires the formation of a ferrous oxyheme. Kinetically, the process is thus usually characterized by the autoxidation rate constant (k_{ox}) which is the first order rate constant of the process at saturating oxygen pressure ($p_{O_2} > p_{50}$).[5−8] The resulting rates have been shown to be strongly dependent on the Mb source (i.e., residue composition)[9,10] as well as on temperature and pH.[11] For sperm whale wild type (wt) Mb, k_{ox} shows a strong "V" shaped pH dependence, increasing ca. 3 orders of magnitude from the minimum at pH 9 to pH 5 and about 150 times from pH 9 to pH 12.[12] This shape of the pH dependence is shown in most studied globin cases, although with variations in the increasing rate. In some cases, loss of either the acid or basic effect is observed, as in the case of denatured bovine heart Mb, where there is no rate increase at acidic pH values.[12]

Received: September 16, 2014
Revised: December 5, 2014
Published: January 12, 2015

DOI: 10.1021/jp5093948
J. Phys. Chem. B 2015, 119, 1802−1813

Scheme 1. Possible Reactions for Oxygen-Mediated Heme Oxidation

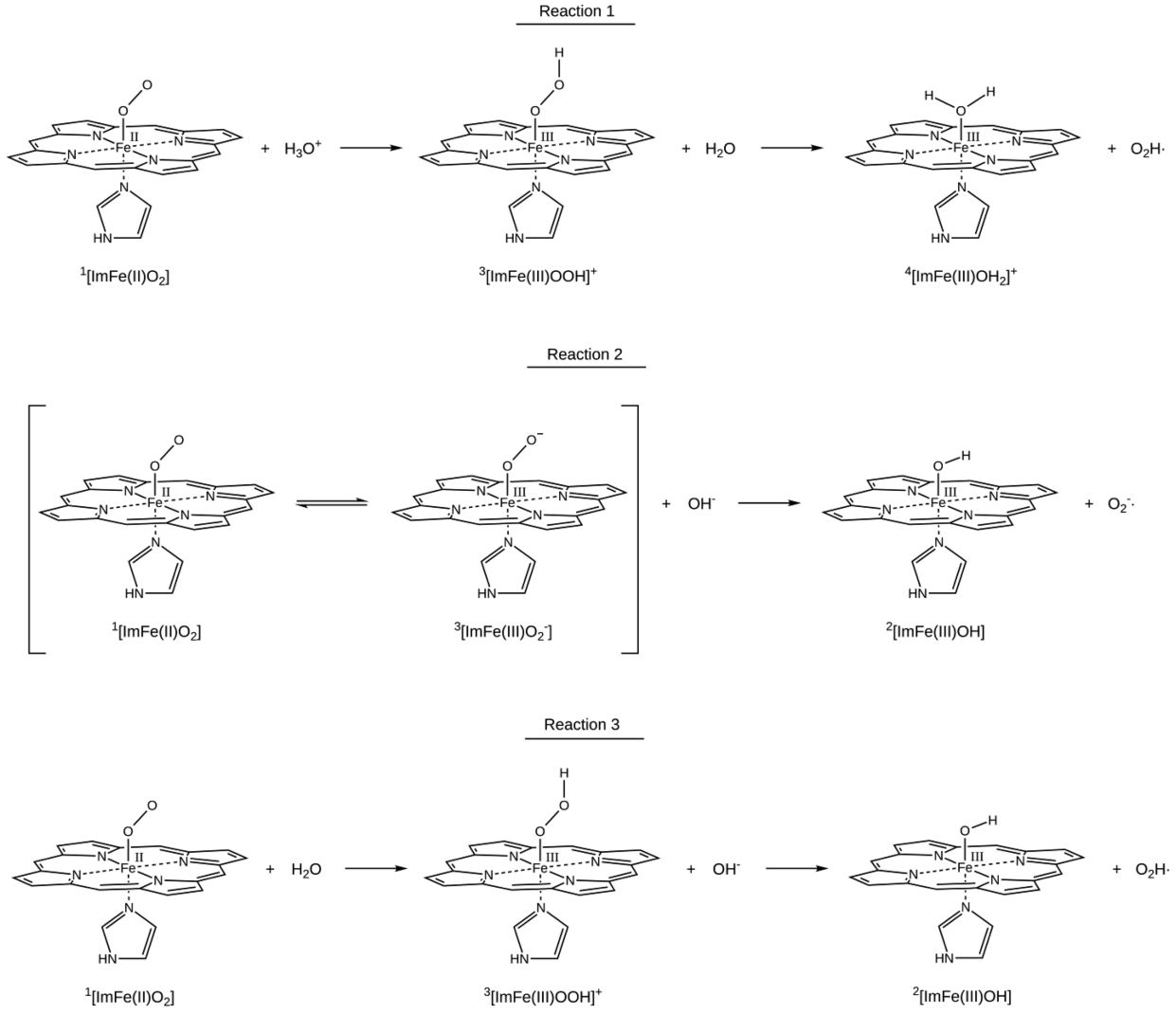

A systematic analysis on how the protein matrix modulates autoxidation rate was also performed using site directed mutants. Mutations that alter the size of the distal pocket (DP) by changing Leu at position 29 (LeuB10) to smaller (L29A) or larger (L29F) hydrophobic residues have shown a significant impact on k_{ox}, with larger DP showing higher rates.[13] The role of the key His64(E7) residue, which is directly involved in heme bound O_2 stabilization, has also been explored extensively and experimental determinations for the H64A, H64Q, and H64F mutants have been reported.[3,14] Interestingly, the values are in all cases larger than those reported for the wt protein, with the alanine mutant displaying an extremely fast autoxidation rate[14] (see Table 3).

The mentioned studies led to several proposals of the underlying mechanism of heme protein autoxidation, presented in Scheme 1. In contrast to iron porphyrins in solution, for which the process is thought to involve a μ-oxo dimer,[15] in proteins the reaction starts with the oxy form of the heme and necessarily involves release and/or displacement of a superoxide (O_2^-) type of ligand. The "V" shaped pH dependence suggested that both acid and base mediated mechanism could be operative. In the first case, protonation of bound oxy−heme results in a Fe(III)−OOH complex, that releases a neutral superoxide radical (OOH·) and possibly binds water forming the readily observed Fe(III)−aquo complex[16] (reaction 1 in Scheme 1). In the base promoted mechanism, the OH^- anion displaces the iron bound superoxide anion (O_2^-) forming a ferric hydroxo complex[11,17] (reaction 2 in Scheme 1). Support for this mechanism also comes from studies using other anions to displace the superoxide which show a positive correlation between the observed rate constant and the conjugated acid pK_a.[17] The acid enhanced mechanism is tightly related to the presence of HisE7, since only proteins bearing this residue show strong proton-catalysis.

In order to shed light on the molecular basis of the possible autoxidation pathways, we decided to perform a detailed study of the processes using a combination of quantum mechanics (QM), molecular dynamics (MD), and hybrid quantum mechanics/molecular mechanics (QM/MM) computer simulation methodologies, taking Mb as the benchmark protein. For this sake, we studied the intrinsic energetics of the reaction in an isolated heme model in vacuum and systematically analyzed the oxy−heme structure and dynamics for wt Mb and five single mutants that either change the DP size or the key HE7 residue. The effects of these mutated residues on the autoxidation reaction energetics were also analyzed. Our results show that superoxide displacement by nucleophiles is more likely to be operative compared to oxy−heme protonation. In

DOI: 10.1021/jp5093948
J. Phys. Chem. B 2015, 119, 1802−1813

addition, the autoxidation rate is enhanced by distal pocket solvation and prevented by the presence of hydrogen bonding interactions between the protein matrix and the bound oxygen ligand. Finally, we show that most of the observed acid catalysis is related to HisE7 opening motion and not to its proton relay capabilities.

THEORETICAL METHODS

Classical Molecular Dynamics Simulations. Each initial structure was built starting with the X-ray model deposited in the Protein Data Bank (PDB) database under the code 1MBO, which corresponds to the sperm whale myoglobin (Mb) in the presence of O_2 as a ligand bound to the heme Fe atom. Distal histidine E7 (H64) was considered protonated in Nε_2 (HIE form) and the proximal histidine was protonated in the Nδ_1 (HID form) and bonded to the heme Fe atom.

The model was fully solvated with an octahedral box of TIP3P water model with periodic boundary conditions. The molecular dynamics (MD) simulations were performed using Amber11 program package.[18] The structure was subjected to a 3-stage protocol before production run: first, side chains optimization with backbone fixed; second, thermalization with a Berendsen thermostat at constant volume until a constant temperature of 300 K was reached; and third, equilibration at constant temperature (300 K) and pressure (1 atm, isotropic position scaling algorithm) to adjust final density. Finally, 100 ns of MD simulation were performed with a time step of 2 fs under the NPT ensemble (constant number of particles, pressure and temperature). A total of 10 000 frames were saved to represent the system movement along the whole simulation time.

Heme parameters for the MD simulations were obtained from QM calculations of the corresponding porphyrin-ligand in vacuum, in combination with a charge fitting procedure and careful calibration with experimental data. The force field parameters are available as Supporting Information and key parameters are shown in Tables S1 and S2. They have been thoroughly validated and used by our group in a wide variety of heme proteins displaying different distal environments.[19]

In preliminary runs of 50 ns, the His64 remained tightly bound through an hydrogen bond to the O_2 along the time scale of the MD simulations. Thus, a restraint to the dihedral angle of its side chain was imposed to remain fixed around 160° (open conformation) instead of 60° (closed conformation) in order to let water molecules enter the distal pocket. In this way, our simulations sampled adequately the situation in which water can access the distal cavity.

We have also computed the free energy profiles for this histidine opening motion using umbrella sampling. The chosen reaction coordinate was the dihedral angle C−Cα−Cβ−Cγ which was set in 60° for the closed conformation and in 160° for the open state. This 100° range was swept in 10 consecutive windows, with symmetric hardness for both sides that ensured an adequate overlapping of the resulting histograms of position frequency.

Radial Pair Distribution Function and Its Integration. The radial pair distribution function, $g(r)$, was centered in the distal atom of the O_2 molecule bound to the heme Fe atom. Water molecules were monitored by its oxygen atom. The increment was set in 0.1 Å and the distance range was 0−30 Å. Finally, a standard normalization procedure was employed. The integration of the $g(r)$ was calculated along the whole range sampled. The useful range of this calculation was established up to the first valley after the first peak, ca. 4 Å.

pK_a Calculations through Constant pH Molecular Dynamics. pK_a calculations were done for wt, L29A, and L29F Mb. Initial structures were taken from their respective MD equilibrated structure with implicit water. Special attention was paid to the HisE7 (closed conformation). All water molecules were removed from the initial structures and an implicit solvation water model was used (the modified generalized Born model developed by Onufriev, Bashford, and Case[20]). To keep tertiary structure, a positional restraint of 1 kcal/Å was applied on the Cα atoms during the time scale of the simulation. The constant pH method implemented in sander (Amber package) addresses these issues through Monte Carlo sampling of the Boltzmann distribution of protonation states concurrent with the molecular dynamics simulation.[21] The nature of the distribution is affected by solvent pH, which is set as an external parameter. Residue protonation states are changed by changing the partial charges on the atoms of the protonable residue. Steepest descent algorithm was used for 1000 minimization steps. The systems were heated up gently from 0 to 300 K in 0.2 ns. The motion equations were integrated with a 2 fs step with a nonbonded cutoff of 40 Å. Three ns of MD simulation at 300 K were done for each of the 8 studied pH (5.0, 5.5, 6.0, 6.5, 7.0, 7.5, 8.0, and 8.5). From each pH simulation, the probability (0 to 1) of having the HisE7 residue with a positive charge was obtained. These values were plotted against pH. The pK_a value was extracted from the extrapolation at probability of 0.5. The method was successfully used in previous works from our group.[22]

Electronic Structure Calculations: Quantum and QM/MM Methods. The model systems for electronic structure calculations were defined as a porphyrin core without side chains, a coordinated imidazole and the corresponding bound ligand. VMD[23] program was used for their preparation. Starting structures for QM/MM calculations were taken from the corresponding classical MD simulations, after slowly (200 ps) cooling of selected snapshots to 0 K.

All QM/MM calculations were optimizations performed with a conjugate gradient algorithm, at the DFT level using the SIESTA code with our own QM/MM implementation called Hybrid.[24] In this method, the quantum and the molecular mechanics subsystems are combined through a hybrid Hamiltonian introducing a modification of the Hartree potential and a QM/MM coupling term. The classical environment affects the electronic density in a self-consistent fashion due to the addition of the classical point charge potential to the Hartree potential. The coupling term has two main contributions representing the electrostatic interaction between the electrons and nuclei, defining the QM charge density with the classical point charge, and an additional term corresponding to the van der Waals and short-range repulsive interactions between the atoms in the quantum and classical regions through a 6-12 Lennard-Jones potential.[24] For all atoms, basis sets of double-ζ plus polarization quality were employed and all calculations were performed using the generalized gradient approximation functional proposed by Perdew, Burke and Ernzerhof (PBE).[25] Only residues located within 10 Å from the heme reactive center were allowed to move freely in the QM/MM runs. The interface between the QM and MM portions of the system was treated with the scaled position link atom method. For all systems studied, the spin-unrestricted approximation was used. The different QM

DOI: 10.1021/jp5093948
J. Phys. Chem. B 2015, 119, 1802−1813

Table 1. Energy Changes Associated to Reactions 1 (* Second Step Only), 2 and 3 Shown in Scheme 1 and Proton Affinities for Heme-Bound Oxy and Hydroxy Complexes[a]

	reaction	ΔE (kcal/mol)
1*	$^3[ImFe(III)O_2H]^+ + H_2O \rightarrow {}^4[ImFe(III)OH_2]^+ + O_2H^\bullet$	+16.2
2	$^1[ImFe(II)O_2] + OH^- \rightarrow {}^2[ImFe(III)OH] + O_2^{-\bullet}$	−13.0
3	$^1[ImFe(II)O_2] + H_2O \rightarrow {}^2[ImFe(III)OH] + O_2H^\bullet$	+24.9
	reaction	proton affinities (kcal/mol)
	$[ImFe(II)O_2] + H^+ \rightarrow [ImFe(III)O_2H]^+$	−237
	$[ImFe(III)OH] + H^+ \rightarrow [ImFe(III)OH_2]^+$	−245

[a]The left superscript number refers to the species spin multiplicity.

subsystems included the heme group (without side chains), the heme ligand (depending on the species to be simulated in each case) and the imidazole group of the proximal histidine. The rest of the protein unit and water molecules were treated classically. QM/MM methods have been successfully applied for the study of heme proteins. Particularly, the Hybrid method showed excellent performance for medium and large systems, and was proven to be appropriate for biomolecules, specifically heme proteins, as shown by several works from our group.[19,26,27] For the model studies in vacuum, the same SIESTA (PBE) calculations as above-described were used.

Finally, while analyzing the proton relay mechanism for the HisE7 residue, a restrained optimization QM/MM method was applied to test the proton transfer from the water solvent to the oxy heme through HisE7. We computed the potential energy profile by using energy minimizations along the reaction path between reactant and product states.[24,27,28] For this approach, an additional term, $V(\xi) = k(\xi - \xi_0)^2$, was added to the potential energy, where k is an adjustable force constant (set to be 200 kcal/mol·Å^2 here) and ξ_0 is a reference value, which was varied stepwise along the reaction coordinate. By varying ξ_0, the system is forced to follow the minimum energy reaction path along the given coordinate. To avoid possible hysteresis problems in the reaction coordinate scan due to accidental changes in the MM part of the system, a distance cutoff of 10 Å was used, this only allows MM atoms that close to the QM active site to move during the scan.

RESULTS

1. QM Calculations of the Autoxidation Mechanism in a Heme Model in Vacuum. We begin our study performing an analysis of the basic reactions involving oxygen mediated heme oxidation, using as a model system an isolated imidazole coordinated iron porphyrin (ImFe) in vacuum. This system has been extensively used as a histidine coordinated heme protein model.[19,26,27,29] The autoxidation reaction can be understood in relation with the two already mentioned acid and base mediated cases, as described respectively by reactions 1 and 2 shown in Scheme 1.

In the first case (reaction 1), the key step is the protonation of the oxy−heme to yield what can be possibly described as a ferric neutral superoxo bound heme, which upon release of the hydrogen superoxide and coordination of water yields a ferric water coordinated heme. In solution, hydroperoxyl radical (pK_a = 4.8)[30] releases the proton to yield the expected superoxide radical anion ($O_2^{-}\cdot$). In the base catalyzed reaction (reaction 2), an hydroxyl anion is proposed to displace a superoxide anion from the heme, a process that possibly involves an oxy−heme electronic redistribution and spin transition to a ferric superoxo state. A third possibility (reaction 3 shown in Scheme 1) can be envisaged combining both limiting cases. Here, a water molecule transfers the proton to the oxy−heme to yield the ferric heme bound to hydrogen superoxide, which is subsequently displaced by the hydroxyl group.

1.1. Autoxidation Reaction Energetics. We computed the energy changes associated with all three reactions shown in Scheme 1 in vacuum (Table 1). For reaction 1, however, only the second step is computed (displacement of the $O_2H^{\cdot}$ by water), since the first step (proton transfer) involves changing the charge of the porphyrin and the ligand and yields unrealistic absolute results in vacuum. Reaction 2, related to base catalysis, is the only exoergic case by −13.0 kcal/mol. The second step of reaction 1 and reaction 3 are both endoergic, displaying values of 16.2 and 24.9 kcal/mol, respectively. The comparison thus shows that water is possibly too weak as a nucleophile to displace the neutral superoxide and a stronger nucleophile such as the hydroxyl group is needed. However, the fact that reaction 3 is endoergic also suggests that the hydroxyl anion displacing force is not enough to compensate the proton transfer from a water molecule to the bound species and that protonation of the oxy heme is quite unfavorable.

1.2. Proton Affinities. The first step of reaction 1 corresponds, as already mentioned, to a proton transfer reaction and it can be understood by analyzing the pK_a of the reacting groups. Although computing accurate pK_as of heme bound ligands is extremely difficult and, as mentioned above, energy calculations for reactions involving change in the total charge of the porphyrin may yield unreliable absolute values, we can analyze some trends by computing and comparing the bound ligand proton affinities. Table 1 shows the proton affinity of the bound oxygen, together with that of an hydroxyl anion ligand for comparison purposes. The results show that the oxy complex proton affinity is 8 kcal/mol smaller than that of the hydroxyl complex. Concerning the hydroxy complex proton affinity, since ferric heme protein crystal structures show examples of both water[31] and hydroxyl coordinated complex,[32] their pK_a values should be consistent with the fact that the two species may exist at the conditions used to grow the crystals. Moreover, water-soluble porphyrins had been shown to display pK_as in the 5−9 range, with most species yielding a pK_a around 5.[33] For the oxy complex a lower pK_a can be expected (for the loss of the proton of its conjugated acid), arguing against the feasibility of the acid catalyzed mechanism.

1.3. Spin States and Geometrical Parameters. Another important point of notice is that in all cases, the presence of a ferric-superoxo (protonated or not) intermediate is crucial for the reaction to take place and that while the starting complex

DOI: 10.1021/jp5093948
J. Phys. Chem. B 2015, 119, 1802−1813

Table 2. Spin States (Noted as Spin Multiplicity with a Left Superscript Number) with Its Energy Differences and Geometrical Parameters for the Porphyrin Complexes Involved in the Autoxidation Reactions Shown in Scheme 1

ground state (GS) complex	^{1}[ImFe(II)−O_2]	^{3}[ImFe(III)−O_2H]$^+$	^{4}[ImFe(III)−OH_2]$^+$	^{2}[ImFe(III)−OH]
first excited spin state (ES)	triplet	singlet	doublet	quartet
$\Delta E_{spin} = E_{ES} - E_{GS}$[a,b]	+1.9	+3.6	+0.8	+14.7
$\Delta E_{spin\text{-}unbound}$[a,c]	+21.2	+22.5	+13.0	+17.6
d_{Fe-O}[d]	+1.84	+1.80	+2.07	+1.83
$q_{L\ GS}/q_{L\ ES}$[e]	−0.23/−0.24	−0.11/−0.09	+0.02/+0.05	−0.35/−0.46
$spin_{Fe\ GS}/spin_{Fe\ ES}$[f]	+0.97/+0.80	+1.27/−0.28	+2.77/+0.98	+0.92/+2.60
$spin_{L\ GS}/spin_{L\ ES}$[e]	−0.90/+1.24	+0.43/−0.24	+0.03/−0.01	+0.19/+0.43

[a]Units of energy are in kcal/mol. [b]ΔE_{spin} is the energy gap between the ground state (GS) and the first excited spin state (ES). [c]$\Delta E_{spin\text{-}unbound}$ is the energy gap between the ground state and the spin state that results in a loose bond or dissociated ligand. [d]d_{Fe-O} is the distance between the heme iron atom and its bound oxygen atom from the ligand. Distance values are in Å. [e]q_L and $spin_L$ are the Mulliken charge and spin population of the bound ligand, respectively. [f]$spin_{Fe}$ is the Mulliken spin population of the Fe atom. Mulliken charge and spin populations are in *e* units.

shows the characteristic diamagnetic singlet spin state, both the intermediate ferric−superoxo and the final ferric−water/hydroxide complex have unpaired electrons. Thus, in all cases the reaction is nonadiabatic and may require a change in the spin state of the heme complex. In this context, it is important to consider that the electronic structure of the Fe(II)−O_2 complex is an open shell singlet, consistently with previous results from Rovira et al.[34] and also those from our group.[35] The zero total spin density is the result of an antiferromagnetic coupling of two regions of opposite spin, centered one on the Fe atom and one on the O_2 ligand, showing spin Mulliken populations of +0.97 and −0.90, respectively. Spin state energetics and spin and charge Mulliken populations of all relevant intermediates are reported in Table 2.

As expected, oxy−heme displays a singlet ground state, with a triplet state lying very close in energy (ΔE = 1.9 kcal/mol). The Mulliken charge population on the ligand is in both cases compatible with a neutral oxygen with only partial superoxide character, although in the triplet state significant unpaired spin density is found in the ligand as expected for superoxide type ligand (spin population of +0.80 on the Fe atom and +1.24 on the O_2 ligand). For higher spin states (quintuplet and septet) where the oxygen can be described as almost unbound (d_{Fe-O} > 2.6 Å), the energy gap is not huge (ΔE < 22 kcal/mol) and the oxygen becomes more neutral ($q_{O_2} \sim -0.1$), consistent with dissociation as molecular oxygen upon electronic excitation. The protonated superoxide complex displays a triplet ground state, with the singlet state close in energy (ΔE = 3.6 kcal/mol). The ligand is almost neutral and with significant unpaired spin density, thus reflecting its $O_2H\cdot$ radical character. The Fe−O distance and the spin gap to the unbound state are similar to those of the oxy−heme and thus a similar bond strength is suggested.

The ferric porphyrin water complex shows a quartet ground state very close to the doublet state (ΔE = 0.8 kcal/mol) and, as expected, a neutral water ligand, while in the ferric−hydroxy complex the doublet ground state is far more stable and the ligand bears a significant negative charge. The spin gap to the unbound state is smaller for the water ligand compared to the hydroxyl, possibly reflecting in part the smaller binding energy of the water complex.

The electronic structure results thus evidence the relevance of the spin transition from the singlet ground state in the initial oxy heme to a triplet state, which is strictly required for the autoxidation to occur, either to increase the population of the ferric−superoxide character state that would allow spin transition and superoxide release, as in the base-catalyzed mechanism, or to establish the ferric−hydrogen superoxide complex with a ground triplet state as in the acid-catalyzed mechanism. In this context, the small spin gap in the oxy−heme is a key element to allow this spin forbidden reaction to take place.

Another interesting point concerns the comparison of the Fe−O distances and energy gaps to the dissociated state, which suggest a similar Fe−O bond strength for the oxy, hydrogen superoxo, and hydroxo complexes, clearly higher than that of the aquo complex. These facts again argue in favor of the base-catalyzed mechanism which turns out to be energetically favored, in comparison with the acid-catalyzed one (Table 1), in part due to the weakly bound aquo complex formed in the latter.

2. MD Analysis of the Active Site Solvation in wt Mb and Its Mutants. Having established the basic energetics of the two proposed extreme cases of heme autoxidation mechanisms (catalyzed by either acid or hydroxide anion, reactions 1 and 2 from Scheme 1 respectively) we will now analyze how they operate in the Mb protein. For this sake, we studied wt Mb; two distal pocket (DP) size mutants L29F and L29A, which respectively show decrease and increase in the autoxidation rate constant compared to the wt protein; and three distal HisE7 mutants (H64A, H64Q and H64F) which also show significant differences in their autoxidation rates (see Table 3).

Table 3. Values of k_{ox}, k_{on} for O_2 and k_{off} for O_2, for Sperm Whale Wild Type Myoglobin and Selected Mutants, Extracted from the Literature

Mb variant	k_{ox} (h^{-1})	k_{on} O_2 (μM^{-1} s^{-1})	k_{off} O_2 (s^{-1})	reference
wt	0.055	16	14	13
L29A	0.24	14	18	13
L29F	0.005	21	1.4	13
H64A	58	53	2300	14
H64Q	0.21	24	130	3
H64F	6	75	10000	14

2.1. Active Site Solvation and Dynamics of wt Mb and Distal Pocket Size Mutants. As previously introduced and required for both mechanistic proposals, our working hypothesis is that the presence of water molecules in contact with the bound oxygen ligand is a key issue to understand the molecular mechanism of autoxidation. To analyze solvation structure and dynamics of Mb, we performed explicit water molecular dynamics (MD) simulations of wt Mb and selected

DOI: 10.1021/jp5093948
J. Phys. Chem. B 2015, 119, 1802−1813

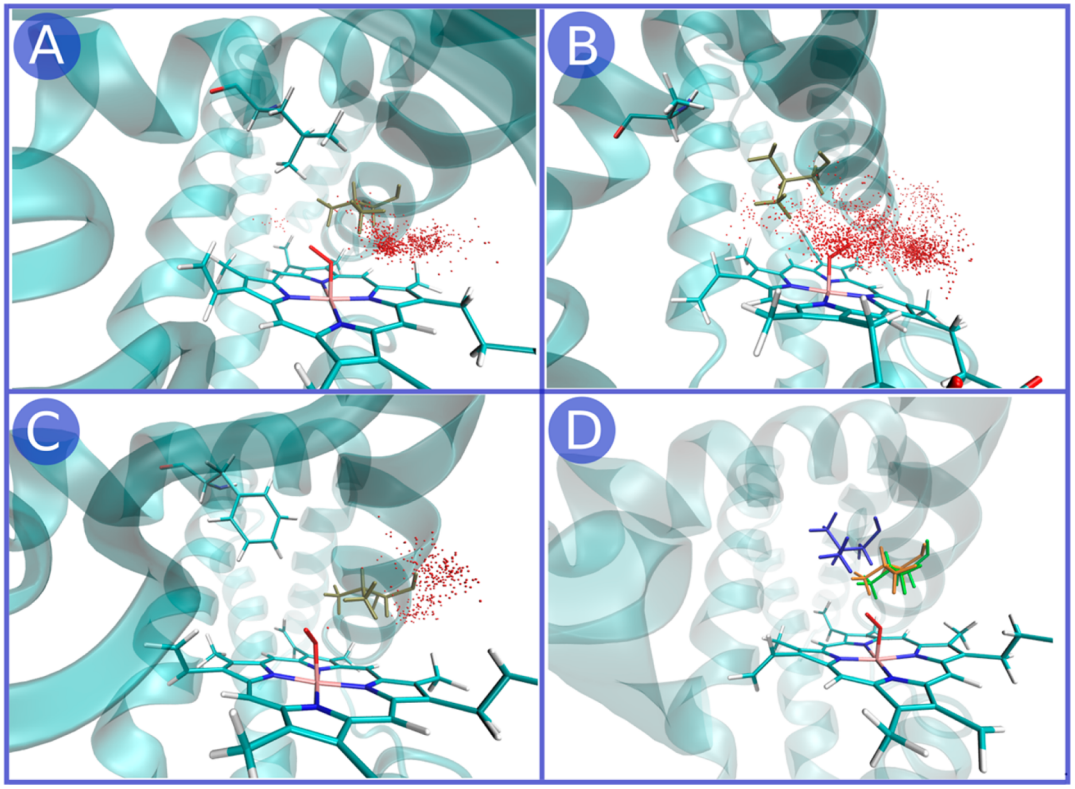

Figure 1. Water distribution patterns in the distal pocket along the molecular dynamics simulation for wt (panel A), L29A (panel B) and L29F (panel C) Mb, all in the open E7 conformation. For sake of clarity water oxygen atoms were represented every 10 ps along the last 50 ns of the MD simulation. The mutated residue of the DP is shown alongside with the Val68 residue. Panel D shows the representative conformation of the E-α helix and the Val68 residue along the MD for wt Mb (orange), L29A (blue), and L29F (green).

distal pocket size Mb mutants (L29A and L29F). Results for wt Mb and the two distal pocket mutants show that when HisE7 is in the closed state, water cannot enter the DP. As already noted by Perutz over 40 years ago[36] HisE7 must change its conformation to allow ligand entrance. Thus, as in our previous work,[37] we analyzed whether water molecules would enter inside the DP when HisE7 is in the open state. In this case, if a restraint is applied to the HisE7 residue in order to keep its open conformation during the simulation (see Methods for details), water molecules are able to enter the DP and remain forming hydrogen bonds with the oxy−heme. Moreover, significant differences in the solvation patterns are observed for each protein variant. Figure 1 shows the water molecule distribution in wt (panel A), L29A (panel B) and L29F (panel C) Mb during the last 50 ns of simulation, with HisE7 in the open conformation. The picture clearly shows that presence of water molecules inside the DP decreases in the following order: L29A > wt (L29) > L29F. It is interesting to notice that the increase in the water penetration inside the DP for L29A is accompanied by a small shift of the E-α helix toward the DP, evidenced by a partial insertion of Val68 residue into the free space left by the L29A mutation (see Figure 1, panel D).

In order to further characterize the solvation structure, we computed for each of the three simulations the radial distribution function of the water oxygen atoms with respect to the outer oxygen atom of the heme bound dioxygen (Figure 2A) and its corresponding integral. Data presented in Figure 2, panel A, clearly show that in all cases the peak corresponding to the first solvation shell is present (at ca. 3 Å), while a second small peak is observed at ca. 5.5 Å only for L29A and wt Mb. In agreement with the visual analysis, the peak height and the integral value including the first solvation shell show that presence of water molecules decreases in the order L29A ≫ wt (L29) > L29F, with wt and L29F mutant being more similar between them. The integral values also allow estimation of average number of water molecules (or the occupancy) that are in contact with the oxy−heme: for L29A Mb the integral value is very close to 1, while it is only 0.3 and 0.2 for wt and L29F respectively.

Since solvation of the DP in wt Mb and mutants is only possible when HisE7 swings out and adopts the open conformation, in order to have a complete picture of the solvation process we analyzed the free energy profiles between the HisE7 in closed and open conformations for all the three systems. The results depicted in Figure 2, panel B, show that in all three cases, as expected, the closed state where the HisE7 is forming an hydrogen bond with the bound oxygen is energetically more favorable. In the wt protein, the open state lies ca. 1 kcal/mol above the closed conformation and a 2 kcal/mol barrier is observed. The L29F shows a similar picture, but with both the barrier and open conformation ca. 1 kcal/mol higher in energy compared to the wt case, a difference possibly originated in the HisE7−F29 aromatic interactions. In L29A Mb, the barrier is significantly higher (ca. 5 kcal/mol) and the open conformation is ca. 2.5 kcal/mol higher in energy than the closed state.

Also important for the opening of the HisE7 residue is its pK_a, since protonation promotes the opening, as observed in the low pH Mb crystal structure[38] and in previous works from our group on the subject.[37] We confirmed the open preference of the protonated HisE7 by computing the corresponding free energy profile (shown in Figure 2B) which clearly shows that

DOI: 10.1021/jp5093948
J. Phys. Chem. B 2015, 119, 1802−1813

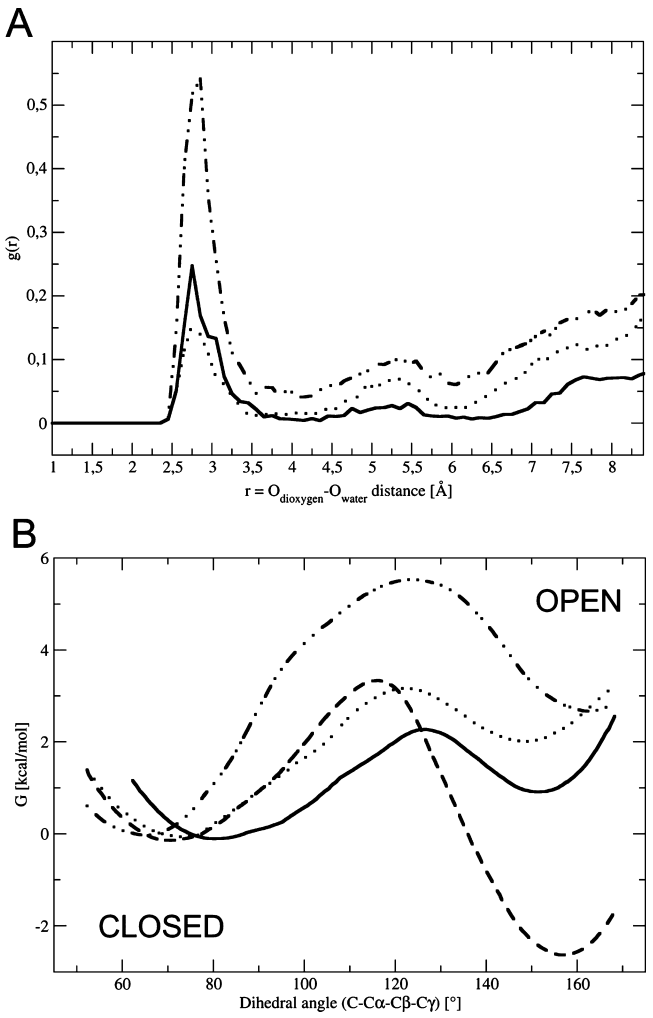

Figure 2. (A) Degree of heme oxygen solvation measured by radial distribution function, $g(r)$, for wt (full line), L29A (dotted–dashed line) and L29F (dotted line) Mb. (B) Free energy profiles for HisE7 in–out interconversion for wt (full line), L29A (dotted–dashed line) and L29F (dotted line) Mb, HisE7 being in Nε protonated form. HisE7 double protonated (in Nε and Nδ) wt Mb was also calculated (dashed line). See text for details.

the open state is energetically favored by ca. −2.5 kcal/mol. Thus, to complete the analysis of the DP mutants, we computed for each protein the HisE7 pK_a using constant pH MD simulations (see Methods for details). The results show that mutations in the DP do not change the HisE7 pK_a dramatically, although increasing it slightly, yielding values of 6.5, 6.9, and 7.2 for wt, L29A and L29F proteins, respectively. The values are compatible with the presence of significant population of the protonated HisE7 at physiological pH of ca. 7. Taking the results of the opening free energy profiles and pK_a calculations together, similar open-closed populations are expected for all three proteins, since the increase in the free energy of the open conformation for the mutants could be compensated by the observed increase in the HisE7 pK_a.

In summary, the results of the DP mutants show that for all proteins similar populations of the open and closed HisE7 states can be expected, with significant population of the open state that allows water molecules to enter the DP. The solvent structure analysis, on the other hand, shows that while L29F protein presents a decrease in the amount and solvation structure around the oxy–heme with respect to wt Mb, the opposite trend is observed for L29A where significant solvent structure is observed in its DP. These results strongly suggest that the amount and structure of water molecules inside the DP is critical for the autoxidation rate, consistently with the experimental k_{ox} values (Table 3).

2.2. Active Site Solvation and Dynamics of HisE7Mb Mutants. We now turn our attention to the solvation and dynamics of HisE7Mb mutants. We performed explicit water MD simulations, and the same analysis described previously, for three Mb mutants, H64A, H64Q and H64F, without restraining the E7 residue conformation. This resulted in a predominant closed conformation for QE7 and FE7 and solvation of the DP and the oxy–heme seemed almost completely blocked in these cases. Again, as for the wt Mb, it is important to note that the E7 residue can adopt an open conformation. We thus performed additional MD simulations with FE7 and QE7Mb in the open state. Figure 3, panel A, shows the corresponding radial distribution functions for these last cases. The plot clearly

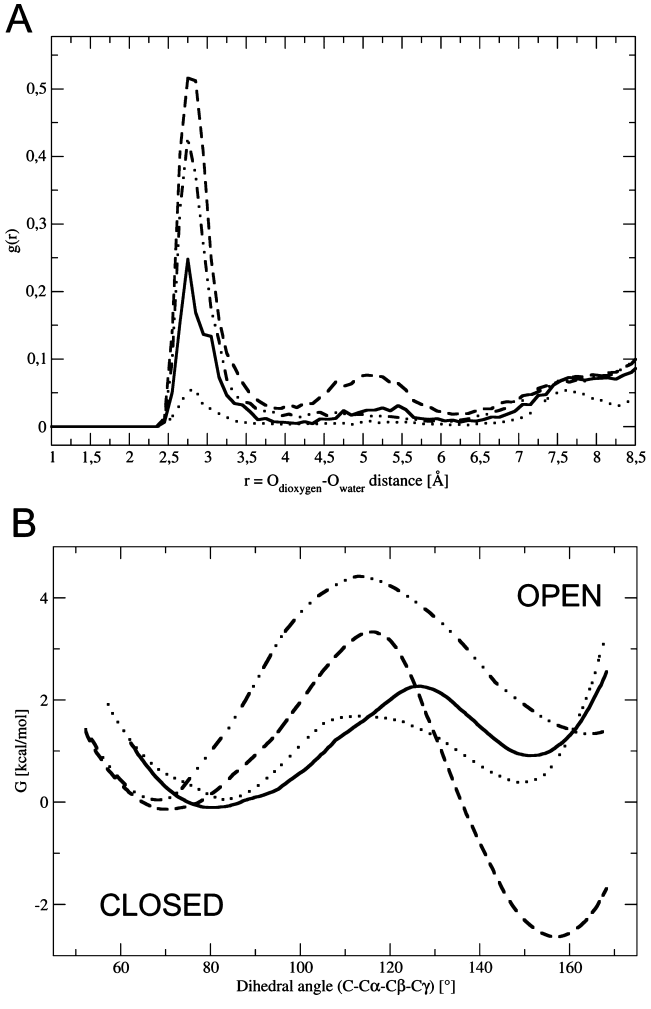

Figure 3. (A) Degree of heme oxygen solvation measured by radial distribution function, $g(r)$, for wt Mb (full line) and its E7 mutants: H64A (dashed line), H64Q in its open conformation (dashed-dotted line) and H64F in its open conformation (dotted line). (B) Free energy profiles for E7 residue in–out interconversion for wt (full line), H64Q (dashed–dotted line), and H64F (dotted line) Mb. HisE7 double protonated (in Nε and Nδ) wt Mb profile is also shown (dashed line).

DOI: 10.1021/jp5093948
J. Phys. Chem. B 2015, 119, 1802–1813

Table 4. Energy Changes Associated with Different Reactions Involving Protein Matrix through QM/MM Calculations[a]

system	wt Mb H64 closed	wt Mb H64 open	H64A Mb	H64Q Mb closed	H64F Mb closed
ΔE reaction 1[b]	+19.1	+20.2	+23.4	+18.9	+16.6
ΔE reaction 2[c]	−16.0	−14.6	−12.9	−13.5	−12.7
ΔE O_2[d]	−28.4	−25.5	−18.9	−28.4	−26.9
ΔE O_2^-[e]	−164.1	−125.2	−140.9	−146.3	−112.1
ΔE O_2H[f]	−32.0	−27.3	−23.7	−31.1	−26.3
Fe−O_2 proton affinity	−240.4	−273.9	−283.7	−257.3	−286.7

[a]Units are all in kcal/mol. [b]ΔE reaction 1 is the energy change associated with the second step of reaction 1 from Scheme 1. [c]ΔE reaction 2 is the energy change associated with reaction 2 from Scheme 1. [d]ΔE O_2 is the oxygen binding energy for the protein relative to its deoxy form and an isolated oxygen molecule in vacuum. [e]ΔE O_2^- is the superoxide binding energy for the protein relative to its deoxy met form and an isolated superoxide ion in vacuum. [f]ΔE O_2H is the hydroperoxyl binding energy for the protein relative to its deoxy met form and an isolated hydroperoxyl radical in vacuum.

shows that when HisE7 is replaced by Ala, a significant amount of water molecules enter the DP and the oxy−heme is completely solvated. Careful visual analysis and determination of the corresponding radial distribution function for the other two E7 mutants restrained in an open conformation shows that in these cases water penetrates the DP and interacts with the bound ligand to different extents. In the H64Q open state, water presence is similar to that of the H64A mutant, while for the H64F only a small number of water molecules enter the DP. This is not unexpected, given the hydrophobic nature of the Phe side chain.

We also computed the free energy profile required for opening the QE7 and FE7 residues (Figure 3, panel B). The H64Q mutant shows a similar free energy difference between the open and closed conformation compared to wt Mb, but presenting a higher barrier of ca. 4 kcal/mol. On the other hand, the H64F mutant shows practically no free energy difference between the open and the closed conformations and a low barrier of less than 2 kcal/mol between both states.

In summary, HE7A mutant shows a highly solvated active site. HE7Q DP is also highly solvated but only in the open state, whose population is similar to that of wt Mb. Finally, although HE7F in open conformation is accessible, water molecules hardly enter the active site.

3. QM/MM analysis of the Autoxidation Reaction in wt Mb and Its Mutants. The previous sections dealt first with the chemical or reactive aspects of the autoxidation reaction, while the second allowed us to perform an analysis of the solvent (the main reactant) structure and dynamics in the selected protein cases. We now perform a final analysis that seeks to combine the previous data by performing a QM/MM analysis of the chemical reaction steps in selected representative structures obtained from the dynamic analysis.

3.1. Energetic Analysis of Ligand Displacement Reaction. Table 4 presents energetic properties for selected protein-states. DP size mutants (L29A and L29F) yielded similar results to those obtained for wt Mb in its HisE7 closed conformation and thus are not shown. The results show two interesting observations. First, the comparison between the base catalyzed displacement of superoxide anion (reaction 2) and the water displacement of hydrogen superoxide (second step of reaction 1) shows that the protein matrix does not significantly affect the fact that base catalyzed mechanism is exoergic, while the other is endoergic. The second aspect is related to those cases where an hydrogen bond is present between the protein and the ligand (wt and H64Q Mb with E7 in its closed conformation) with respect to those where there is none (wt with E7 in open conformation, H64F and H64A Mb). Several kinetic[3,13,39,40] and theoretical studies[26,41−43] have shown that distal protein formation of hydrogen bond significantly stabilizes the oxygen bound ligand. This results in larger oxygen binding energies (ΔE O_2) as shown in Table 4 and is reflected in small k_{off} values (see Table 3). H64A and H64F mutants, on the contrary, show very high dissociation rates and smaller binding energies. This distal stabilization of the bound ligand also results in larger energy required to release the superoxide anion or the hydroperoxyl radical. Thus, presence of hydrogen bond is expected to reduce k_{ox} by retaining the bound ligand in both mechanisms.

3.2. Proton Affinity Analysis. Regarding the acid catalyzed autoxidation mechanism, we also computed the proton affinity of the bound oxygen ligand (first step of reaction 1, Scheme 1). The results presented in Table 4 show again the key role played by the hydrogen bond to the bound ligand. The presence of the hydrogen bond reduces the proton affinity (compare wt *closed* or H64Q Mb with wt *open*, H64A or H64F Mb).

In summary, the QM/MM results for the different protein states again suggest a major role for the basic catalyzed mechanism and point toward protection against autoxidation by means of distal hydrogen bond interactions.

DISCUSSION

To fully understand the underlying mechanism of heme protein autoxidation, it is important to analyze the extensive amount of experimental results obtained through many years of intensive work done mainly by the groups from Shikama[9,12,44,45] and Olson[6,46−48] who measured autoxidation rates (among other properties) of many wt and mutant globins from different sources and in a wide range of conditions. Given the complexities of the reaction we will separately analyze the different structural and reactivity contributions that determine a given heme protein autoxidation rate. The first important point to be drawn concerns the relation between k_{ox} and the oxygen pressure. Previous works by the mentioned groups clearly show a k_{ox} vs p_{O_2} plot with a complex behavior: the k_{ox} increases under low oxygen pressure up to maximum rate which closely corresponds to the oxygen pressure required to half saturate the protein, that is to say p_{50}; then k_{ox} decays until a constant value is reached. This behavior is usually interpreted in terms of a dual mechanism, which can be described through a bimolecular reaction between the protein and O_2 under low oxygen pressure, and a unimolecular reaction of the oxy−protein dominant under $p_{O_2} > p_{50}$. Our work focuses on the mechanism related to the unimolecular reaction, which corresponds to autoxidation of the oxygenated heme.

DOI: 10.1021/jp5093948
J. Phys. Chem. B 2015, 119, 1802−1813

A critical event in the autoxidation process is the transfer of an electron from the Fe(II) center to the bound dioxygen ligand. Thermodynamically, the reaction is governed by the corresponding heme redox potential that, although showing significant variation among heme proteins, is always higher than that of the oxygen/superoxide couple, and usually lies in the range 0.02−0.06 V, at pH 7, for myoglobin from different sources.[49−51] Concerning the pH dependence, sperm whale myoglobin redox potential remains practically constant around 0.05 V between pH 6−8 and shows a small linear decrease above pH 8, until it reaches a value of −0.05 V at pH 10.5.[52] Thus, for Mb, autoxidation becomes slightly more favorable above pH 8. On the other hand, dioxygen reduction to superoxide anion (pK_a = 4.8[30]) is possibly pH independent at physiological and higher pHs, showing a redox potential of −0.33 V.[53,54] However, for low pH (close and below superoxide pK_a) there is a significant amount of neutral (protonated) superoxide radical, and the reduction potential for the couple $O_2/HO_2\cdot$ is expected to be higher than that of $O_2/O_2^{-}\cdot$,[55] thus also promoting the autoxidation reaction. In summary, from a pure thermodynamic electrochemical viewpoint, the autoxidation reaction is expected to be favored above pH 8 and close to pH 5, following the same trend as experimentally observed (see below).

Role of H64 Opening in Acid Catalysis. When analyzing wt Mb (as well as many other globins) autoxidation rates as a function of the environment pH, a characteristic inverted bell shaped curve is evidenced, which is indicative of both acid and base assisted catalysis. For wt Mb for example, k_{ox} at pH 8−9 is ca. 10^{-3} h^{-1}, and increases 3 orders of magnitude at pH of ca. 5, and about 150 times at pH 12.[12] At first sight our results seem at odds with these observations since both our reaction energy and oxy−heme proton affinity analysis suggest that basic superoxide anion releasing mechanism should be favored. However, key to the present analysis is the behavior of the distal H64. The acid-enhanced mechanism is tightly related to the presence of this residue, since only proteins bearing H64 show strong proton-catalysis. The role of H64 in Mb is complex since it exhibits a pH dependent conformational behavior that modulates entry to the DP (the so-called HisE7 gate[36]).[56] As shown by several experimental[57] and theoretical works,[37] HisE7 exists not only in a closed conformation where it partially blocks the DP access and can interact with the heme bound ligands, but also in an open solvent exposed conformation that promotes small ligand access to the DP. The equilibrium between open−closed conformations is strongly dependent on the His tautomeric and protonation state, with positively charged HisE7 favoring the open conformation. Our results clearly show that only when H64 is in the open conformation, water molecules can enter the DP to protonate and displace the ligand. Thus, the observed increase in the k_{ox} rate when the pH is lowered could be due to an increase in the population of the H64 open state. This interpretation is consistent with the observations made by Shikama et al. of H64 Mb mutants which show smaller increase with lower pH. For example, H64L/V/G mutants show only a ca. 10 times increase when moving from pH 9 to 4 (compared to 10 000 times increase observed for wt Mb). Moreover, denatured Mb completely looses the acid catalysis while retaining the basic one.[12] Indeed Shikama et al. explicitly stated that "At any rate, our detailed pH-dependence studies for a dozen of myoglobins isolated from various sources have shown that only the proteins having the usual distal (E7) histidine residue can manifest a very strong proton-catalysis in the autoxidation reaction".[9,58,59] In summary, our data strongly suggest that a significant part of the observed acid catalysis resides in the H64 capacity to become protonated promoting its opening and allowing water molecules to enter the DP and displace the superoxide ligand.

Oxy−Heme Protonation Role in Acid Catalysis. Protonation of the oxy−heme has been proposed to play two roles in the context of the autoxidation reaction. First, it was related to the fact that a neutral protonated superoxide would be easier to dissociate from the ferric heme than a negatively charged superoxide anion. Although this seems a reasonable rule of thumb, it fails to account for the fact that autoxidation reaction is not a simple dissociation but requires displacement either by a water, hydroxyl or other ferric heme ligand (see below for further analysis of this point). The other is related to the role of H64 in its closed conformation, which in acid catalysis could act as proton donor or relay shuffling protons from the solvent to the bound ligand,[60−62] yielding an alternative explanation for its key role to our above-mentioned proposal.

Concerning the first point, our QM and QM/MM results for the whole reaction energetics suggest that water displacement of the neutral superoxide is far less favorable than superoxide anion displacement by hydroxyl. Also, spin state and geometry analysis suggest that intrinsic Fe−O bond strength is similar for O_2H and O_2. However, it is important to note that superoxide anion releasing mechanism is spin forbidden and requires transition from low to high spin of the oxy heme. On the other hand, protonation of oxy−heme fixes the complex in a high spin conformation thus facilitating the reaction and possibly explaining the rate enhancement at low pH.

Concerning the second point, we tested the reaction coordinate of transferring a proton from an outer water molecule to the heme bound oxygen through the H64 (relay mechanism) by means of QM/MM restrained optimization (see Methods), obtaining a very high barrier of ca. 34 kcal/mol. The first note is that in order for the H64 being able to protonate oxy−heme, it should display a lower pK_a. Our estimates for H64 pK_a are in the 6−7 range, while proton affinity analysis of oxy−heme suggests it having a lower pK_a than that corresponding to Fe−OH/aquo. Although there are no pK_a values calculated for this aquo complex in a globin protein environment, in most water-soluble porphyrins it had been shown to possess a pK_a value lower than 7.[33] Moreover, when H64 is protonated, it opens up and thus its interaction with the bound ligand is absent. Finally, concerning oxy−heme protonation, it is important to note that any residue forming hydrogen bonds with the bound ligand diminish its capability of accepting the proton.

Ligand Displacement is the Key to Basic Catalysis. Our energetic results suggest that key to basic catalysis is the incoming OH^- ligand binding capacity. Indeed, displacement of superoxide anion by OH^- is significantly more favorable from a pure energetic point of view than hydrogen superoxide displacement by water. The predominant role of the incoming ligand affinity is consistent with studies by Shikama[11] where the k_{ox} was measured in the presence of several anions, including SCN^-, F^-, CN^-, and N_3^- among others. The results showed that $\log(k_{ox})$ vs pK_a (of the conjugated acid of each anion) yields a linear plot with a slope of 1.74, thus evidencing that autoxidation proceeds by way of a nucleophilic attack of the

DOI: 10.1021/jp5093948
J. Phys. Chem. B 2015, 119, 1802−1813

base to the iron, leading to a reductive displacement of the oxygen ligand as superoxide.

Solvation Structure of the Distal Pocket Correlates with Autoxidation Rate. Having analyzed the chemical steps of the autoxidation reaction we now turn our attention to the role played by the protein matrix on its rate, at any given pH value (usually pH 7). As shown in Table 3, significant differences are observed among wt and single point mutant Mb proteins. As in the Results, we can divide the analysis in two cases, those where key H64 is mutated and those retaining it. Looking at the three H64 containing proteins, the k_{ox} trend is as follows: L29F < wt < L29A. Our analysis show that all three proteins are expected to show similar populations of the open-closed states of H64, as well as comparable reaction energetic parameters, the main difference between them being the solvation structure inside the distal pocket (DP), which follows the same trend as shown by the k_{ox} in relation to the amount and structure of the water molecules inside the DP. In other words, while the fast autoxidative L29A protein shows the presence of water molecules all over the DP, in the wt protein the penetration of water to the DP is less defined and in L29F the presence of the hydrophobic side chain only leaves the presence of water close to H64. The fact that k_{ox} is directly related to the amount of water molecules inside the DP, and thus close to the iron and the oxygen, is consistent with the displacement mechanism since waters/OH^- must be there to displace the ligand. In this context, it is important to remark that water molecules, particularly those ones close to H64, are in direct contact with the surrounding solvent and thus could easily release a proton to become an hydroxyl ion.

Distal Pocket Ligand Interactions Significantly Protect the Heme from Autoxidation. Finally, when looking at H64 Mb mutants, the trend for the autoxidation rate is as follows: wt < H64Q ≪ H64F < H64A (see Table 3). Our results show that both wt and H64Q proteins display strong hydrogen bond interactions with the bound ligand which, as shown by the energetic data, results in a higher energy cost that must be paid to release superoxide anion or hydrogen superoxide. This cost has the same origin as that required to release molecular oxygen, as characterized by the k_{off} (Table 3), which is the main factor responsible for determining overall oxygen affinity in globins,[63] as also shown by our energetic data. The role of the distal residues in inhibiting ligand release as a key of the autoxidation process is consistent with the observations performed by Brantley and Olson[3] which show a direct linear relationship between log(k_{ox}) and log(oxygen K_d).

The difference between wt and H64Q as well as that between H64F and H64A can be explained in relation with the above-mentioned solvation properties. H64Q displays a 4-fold faster k_{ox} compared to wt Mb and consistently H64Q shows an increased solvated DP. Again, while H64F shows almost a complete lack of water molecules inside the DP, H64A DP shows the presence of several well-defined sites to allocate water molecules. Last but not least, the fact that moderately DP solvated H64Q and wt Mb show lower k_{ox} values than the almost dry DP of H64F suggest that the role of the distal residue ligand interaction is the dominant effect for protecting oxy−heme from autoxidation.

CONCLUSION

The overall trend of the determined k_{ox} for all proteins studied in the present work is as follows: L29F < wt < L29A = H64Q < H64F < H64A and can only be explained by considering a combination of both distal hydrogen bond interactions and access of solvent to the DP. From both effects the distal interaction seems the most important since all proteins displaying them have lower k_{ox} values, while solvation effects nicely explain the trends in each group.

ASSOCIATED CONTENT

Supporting Information

Heme parameters for performing MD simulations and tables of partial charges and 6-12 potential parameters. This material is available free of charge via the Internet at http://pubs.acs.org.

AUTHOR INFORMATION

Corresponding Authors

*(M.A.M.) E-mail: marcelo@qi.fcen.uba.ar.

*(D.A.E.) E-mail: dario@qi.fcen.uba.ar. Telephone: +54 11 4576 3378 (Int. 123).

Author Contributions

§Both authors contributed equally to this work.

Notes

The authors declare no competing financial interest.

ACKNOWLEDGMENTS

This work has been supported by grants of European Union (FP7 NOSTRESS), Agencia Nacional de Promoción Científica y Tecnológica (PICT 06-1266 and PICT 2010-416), CONICET (PIP 2012-2014 #112 201101 00850), and by Universidad de Buenos Aires. J.P.A. acknowledges Universidad de Buenos Aires and CONICET for undergraduate and doctoral fellowships, respectively, and is deeply grateful to ALN for technical support and invaluable advice.

REFERENCES

(1) Wittenberg, J. B.; Wittenberg, B. A. Myoglobin Function Reassessed. *J. Exp. Biol.* **2003**, *206* (12), 2011−2020.

(2) Sugawara, Y.; Shikama, K. Autoxidation of Native Oxymyoglobin. Thermodynamic Analysis of the pH Profile. *Eur. J. Biochem.* **1980**, *110* (1), 241−246.

(3) Brantley, R. E., Jr.; Smerdon, S. J.; Wilkinson, A. J.; Singleton, E. W.; Olson, J. S. The Mechanism of Autooxidation of Myoglobin. *J. Biol. Chem.* **1993**, *268* (10), 6995−7010.

(4) Zhu, X.; Zuo, L. X. Characterization of Oxygen Radical Formation Mechanism at Early Cardiac Ischemia. *Cell Death Dis.* **2013**, *4*, e787.

(5) George, P.; Stratmann, C. J. The Oxidation of Myoglobin to Metmyoglobin by Oxygen. I. *Biochem. J.* **1952**, *51* (1), 103−108.

(6) Smagghe, B. J.; Hoy, J. A.; Percifield, R.; Kundu, S.; Hargrove, M. S.; Sarath, G.; Hilbert, J.-L.; Watts, R. A.; Dennis, E. S.; Peacock, W. J.; et al. Review: Correlations Between Oxygen Affinity and Sequence Classifications of Plant Hemoglobins. *Biopolymers* **2009**, *91* (12), 1083−1096.

(7) Olson, J. S.; Maillet, D. H. Designing Recombinant Hemoglobin for Use as a Blood Substitute. In *Blood Substitutes*; Winslow, R. M., Ed; Academic Press, Elsevier: Amsterdam, 2006, 354−374.

(8) Kamimura, S.; Matsuoka, A.; Imai, K.; Shikama, K. The Swinging Movement of the Distal Histidine Residue and the Autoxidation Reaction for Midge Larval Hemoglobins. *Eur. J. Biochem.* **2003**, *270* (7), 1424−1433.

(9) Shikama, K.; Matsuoka, A. Aplysia Myoglobin with Unusual Properties: Another Prototype in Myoglobin and Haemoglobin Biochemistry. *Biol. Rev. Cambridge Philos. Soc.* **1994**, *69* (2), 233−251.

(10) Tsubamoto, Y.; Matsuoka, A.; Yusa, K.; Shikama, K. Protozoan Myoglobin from *Paramecium caudatum*. Its Autoxidation Reaction and Hemichrome Formation. *Eur. J. Biochem.* **1990**, *193* (1), 55−59.

DOI: 10.1021/jp5093948
J. Phys. Chem. B 2015, 119, 1802−1813

(11) Shikama, K. The Molecular Mechanism of Autoxidation for Myoglobin and Hemoglobin: A Venerable Puzzle. *Chem. Rev.* **1998**, *98* (4), 1357−1373.
(12) Shikama, K. Nature of the FeO_2 Bonding in Myoglobin and Hemoglobin: A New Molecular Paradigm. *Prog. Biophys. Mol. Biol.* **2006**, *91* (1−2), 83−162.
(13) Carver, T. E.; Brantley, R. E., Jr.; Singleton, E. W.; Arduini, R. M.; Quillin, M. L.; Phillips, G. N., Jr.; Olson, J. S. A Novel Site-Directed Mutant of Myoglobin with an Unusually High O_2 Affinity and Low Autooxidation rate. *J. Biol. Chem.* **1992**, *267* (20), 14443−14450.
(14) Springer, B. A.; Sligar, S. G.; Olson, J. S.; Phillips, G. N., Jr. Mechanisms of Ligand Recognition in Myoglobin. *Chem. Rev.* **1994**, *94* (3), 699−714.
(15) Cohen, I. A.; Caughey, W. S. Substituted Deuteroporphyrins. IV. On the Kinetics and Mechanism of Reactions of Iron(II) Porphyrins with Oxygen. *Biochemistry* **1968**, *7* (2), 636−641.
(16) Ladner, R. C.; Heidner, E. J.; Perutz, M. F. The Structure of Horse Methaemoglobin at 2.0 Å Resolution. *J. Mol. Biol.* **1977**, *114* (3), 385−413.
(17) Satoh, Y.; Shikama, K. Autoxidation of Oxymyoglobin. A Nucleophilic Displacement Mechanism. *J. Biol. Chem.* **1981**, *256* (20), 10272−10275.
(18) Case, D. A.; Cheatham, T. E., III; Darden, T.; Gohlke, H.; Luo, R.; Merz, K. M., Jr.; Onufriev, A.; Simmerling, C.; Wang, B.; Woods, R. J. The Amber Biomolecular Simulation Programs. *J. Comput. Chem.* **2005**, *26* (16), 1668−1688.
(19) Martí, M. A.; Crespo, A.; Capece, L.; Boechi, L.; Bikiel, D. E.; Scherlis, D. A.; Estrin, D. A. Dioxygen Affinity in Heme Proteins Investigated by Computer Simulation. *J. Inorg. Biochem.* **2006**, *100* (4), 761−770.
(20) Onufriev, A.; Bashford, D.; Case, D. A. Modification of the Generalized Born Model Suitable for Macromolecules. *J. Phys. Chem. B* **2000**, *104* (15), 3712−3720.
(21) Mongan, J.; Case, D. A.; McCammon, J. A. Constant pH Molecular Dynamics in Generalized Born Implicit Solvent. *J. Comput. Chem.* **2004**, *25* (16), 2038−2048.
(22) Di Russo, N. V.; Estrin, D. A.; Martí, M. A.; Roitberg, A. E. pH-dependent Conformational Changes in Proteins and Their Effect on Experimental pKas: The Case of Nitrophorin 4. *PLoS Comput. Biol.* **2012**, *8* (11), e1002761.
(23) Humphrey, W.; Dalke, A.; Schulten, K. VMD: Visual Molecular Dynamics. *J. Mol. Graph.* **1996**, *14* (1), 33−38.
(24) Crespo, A.; Scherlis, D. A.; Martí, M. A.; Ordejón, P.; Roitberg, A. E.; Estrin, D. A. A DFT-based QM-MM Approach Designed for the Treatment of Large Molecular Systems: Application to Chorismate Mutase. *J. Phys. Chem. B* **2003**, *107* (49), 13728−13736.
(25) Perdew, J. P.; Burke, K.; Ernzerhof, M. Generalized Gradient Approximation Made Simple. *Phys. Rev. Lett.* **1996**, *77* (18), 3865−3868.
(26) Capece, L.; Boechi, L.; Perissinotti, L. L.; Arroyo-Mañez, P.; Bikiel, D. E.; Smulevich, G.; Marti, M. A.; Estrin, D. A. Small Ligand-globin Interactions: Reviewing Lessons Derived from Computer Simulation. *Biochim. Biophys. Acta* **2013**, *1834* (9), 1722−1738.
(27) Bikiel, D. E.; Boechi, L.; Capece, L.; Crespo, A.; De Biase, P. M.; Di Lella, S.; González Lebrero, M. C.; Martí, M. A.; Nadra, A. D.; Perisinotti, L. L.; et al. Modeling Heme Proteins Using Atomistic Simulations. *Phys. Chem. Chem. Phys.* **2006**, *8* (48), 5611−5628.
(28) Perissinotti, L. L.; Marti, M. A.; Doctorovich, F.; Luque, F. J.; Estrin, D. A. A Microscopic Study of the Deoxyhemoglobin-catalyzed Generation of Nitric Oxide from Nitrite Anion. *Biochemistry* **2008**, *47* (37), 9793−9802.
(29) Petruk, A. A.; Vergara, A.; Estrin, D.; Merlino, A. Molecular Basis of the NO Trans Influence in Quaternary T-state Human Hemoglobin: A Computational Study. *FEBS Lett.* **2013**, *587* (15), 2393−2398.
(30) Bielski, B. H. J.; Cabelli, D. E.; Arudi, R. L.; Ross, A. B. Reactivity of HO_2/O_2^- Radicals in Aqueous Solution. *J. Phys. Chem. Ref. Data.* **1985**, *14* (4), 1041−1100.
(31) Ostermann, A.; Tanaka, I.; Engler, N.; Niimura, N.; Parak, F. G. Hydrogen and Deuterium in Myoglobin as Seen by a Neutron Structure Determination at 1.5 Å Resolution. *Biophys Chem.* **2002**, *95* (3), 183−193.
(32) Hersleth, H.; Dalhus, B.; Görbitz, C. H.; Andersson, K. K. An Iron Hydroxide Moiety in the 1.35 Å Resolution Structure of Hydrogen Peroxide Derived Myoglobin Compound II at pH 5.2. *J. Biol. Inorg. Chem.* **2002**, *7* (3), 299−304.
(33) Jee, J. E.; van Eldik, R. Mechanistic Studies on the Nitrite-catalyzed Reductive Nitrosylation of Highly Charged Anionic and Cationic Fe^{III} Porphyrin Complexes. *Inorg. Chem.* **2006**, *45* (16), 6523−6534.
(34) Rovira, C.; Kunc, K.; Hutter, J.; Ballone, P.; Parrinello, M. Equilibrium Geometries and Electronic Structure of Iron-Porphyrin Complexes: A Density Functional Study. *J. Phys. Chem. A* **1997**, *101*, 8914−8925.
(35) Crespo, A.; Marti, M. A.; Kalko, S. G.; Morreale, A.; Orozco, M.; Gelpi, J. L.; Luque, J.; Estrin, D. A. Theoretical Study of the Truncated Hemoglobin HbN: Exploring the Molecular Basis of the NO Detoxification Mechanism. *J. Am. Chem. Soc.* **2005**, *127*, 4433−4444.
(36) Perutz, M. F.; Mathews, F. S. An X-ray Study of Azide Methaemoglobin. *J. Mol. Biol.* **1966**, *21* (1), 199−202.
(37) Boechi, L.; Arrar, M.; Martí, M. A.; Olson, J. S.; Roitberg, A. E.; Estrin, D. A. Hydrophobic Effect Drives Oxygen Uptake in Myoglobin via Histidine E7. *J. Biol. Chem.* **2013**, *288* (9), 6754−6762.
(38) Vojtěchovský, J.; Chu, K.; Berendzen, J.; Sweet, R. M.; Schlichting, I. Crystal Structures of Myoglobin-ligand Complexes at Near-atomic Resolution. *Biophys. J.* **1999**, *77* (4), 2153−2174.
(39) Scott, E. E.; Gibson, Q. H.; Olson, J. S. Mapping the Pathways for O_2 Entry Into and Exit from Myoglobin. *J. Biol. Chem.* **2001**, *276* (7), 5177−5188.
(40) Goldbeck, R. A.; Bhaskaran, S.; Ortega, C.; Mendoza, J. L.; Olson, J. S.; Soman, J.; Kliger, D. S.; Esquerra, R. M. Water and Ligand Entry in Myoglobin: Assessing the Speed and Extent of Heme Pocket Hydration After CO Photodissociation. *Proc. Natl. Acad. Sci. U.S.A.* **2006**, *103* (5), 1254−1259.
(41) Arroyo-Mañez, P.; Bikiel, D. E.; Boechi, L.; Capece, L.; Di Lella, S.; Estrin, D. A.; Marti, M. A.; Moreno, D. M.; Nadra, A. D.; Petruk, A. A. Protein Dynamics and Ligand Migration Interplay as Studied by Computer Simulation. *Biochim. Biophys. Acta* **2011**, *1814* (8), 1054−1064.
(42) Martí, M. A.; Capece, L.; Bikiel, D. E.; Falcone, B.; Estrin, D. A. Oxygen Affinity Controlled by Dynamical Distal Conformations: The Soybean Leghemoglobin and the *Paramecium caudatum* Hemoglobin Cases. *Proteins: Struct., Funct., Genet.* **2007**, *68* (2), 480−487.
(43) Arroyo-Mañez, P.; Lu, C.; Boechi, L.; Martí, M. A.; Shepherd, M.; Wilson, J. L.; Poole, R. K.; Luque, F. J.; Yeh, S. R.; Estrin, D. A. Role of the Distal Hydrogen-bonding Network in Regulating Oxygen Affinity in the Truncated Hemoglobin III from *Campylobacter jejuni*. *Biochemistry* **2011**, *50* (19), 3946−3956.
(44) Shikama, K. Autoxidation of Oxymyoglobin: A Meeting Point of the Stabilization and the Activation of Molecular Oxygen. *Biol. Rev. Camb. Philos. Soc.* **1990**, *65* (4), 517−527.
(45) Shikama, K. Nature of the FeO_2 Bonding in Myoglobin: An Overview from Physical to Clinical Biochemistry. *Experientia* **1985**, *41* (6), 701−706.
(46) Varnado, C. L.; Mollan, T. L.; Birukou, I.; Smith, B. J.; Henderson, D. P.; Olson, J. S. Development of Recombinant Hemoglobin-based Oxygen Carriers. *Antioxid. Redox Signaling* **2013**, *18* (17), 2314−2328.
(47) Olson, J. S.; Soman, J.; Phillips, G. N., Jr. Ligand Pathways in Myoglobin: A Review of Trp Cavity Mutations. *IUBMB Life* **2007**, *59* (8−9), 552−562.
(48) Olson, J. S.; Phillips, G. N., Jr. Kinetic Pathways and Barriers for Ligand Binding to Myoglobin. *J. Biol. Chem.* **1996**, *271* (30), 17593−17596.
(49) Battistuzzi, G.; Bellei, M.; Casella, L.; Bortolotti, C. A.; Roncone, R.; Monzani, E.; Sola, M. Redox Reactivity of the Heme Fe^{3+}/Fe^{2+}

DOI: 10.1021/jp5093948
J. Phys. Chem. B 2015, 119, 1802−1813

Couple in Native Myoglobins and Mutants with Peroxidase-like Activity. *J. Biol. Inorg. Chem.* **2007**, *12* (7), 951−958.
(50) Taylor, J. F.; Morgan, V. E. Oxidation-reduction Potentials of the Metmyoglobin-myoglobin System. *J. Biol. Chem.* **1942**, *144*, 15−20.
(51) Varadarajan, R.; Zewert, T. E.; Gray, H. B.; Boxer, S. G. Effects of Buried Ionizable Amino Acids on the Reduction Potential of Recombinant Myoglobin. *Science* **1989**, *243*, 69−72.
(52) Brunori, M.; Saggese, U.; Rotilio, G. C.; Antonini, E.; Wyman, J. Redox Equilibrium of Sperm-Whale Myoglobin, Aplysia Myoglobin, and Chironomus thummi Hemoglobin. *Biochemistry* **1971**, *10* (9), 1604−1609.
(53) Wood, P. The Potential Diagram for Oxygen at pH 7. *Biochem. J.* **1988**, *253*, 287−289.
(54) Sawada, Y.; Iyanagi, T.; Yamazaki, I. Relation between Redox Potentials and Rate Constants in Reactions Coupled with the System Oxygen-Superoxide. *Biochemistry* **1975**, *14* (17), 3761−3764.
(55) Rao, P. S.; Hayon, E. Redox Potentials of Free Radicals. IV. Superoxide and Hydroperoxy Radicals $\cdot O_2^-$ and $\cdot HO_2$. *J. Phys. Chem.* **1975**, *79* (4), 397−402.
(56) Akiyama, K.; Fukuda, M.; Kobayashi, N.; Matsuoka, A.; Shikama, K. The pH-dependent Swinging-out of the Distal Histidine Residue in Ferric Hemoglobin of a Midge Larva (*Tokunagayusurika akamusi*). *Biochim. Biophys. Acta* **1994**, *1208* (2), 306−309.
(57) Yang, F.; Phillips, G. N., Jr. Crystal Structures of CO-, Deoxy- and Met-myoglobins at Various pH Values. *J. Mol. Biol.* **1996**, *256* (4), 762−774.
(58) Tada, T.; Watanabe, Y.; Matsuoka, A.; Ikeda-Saito, M.; Imai, K.; Ni-Hei, Y.; Shikama, K. African Elephant Myoglobin with an Unusual Autoxidation Behavior: Comparison with the H64Q Mutant of Sperm Whale myoglobin. *Biochim. Biophys. Acta* **1998**, *1387* (1−2), 165−176.
(59) Suzuki, T.; Watanabe, Y. H.; Nagasawa, M.; Matsuoka, A.; Shikama, K. Dual Nature of the Distal Histidine Residue in the Autoxidation Reaction of Myoglobin and Hemoglobin: Comparison of the H64 Mutants. *Eur. J. Biochem.* **2000**, *267* (20), 6166−6174.
(60) Alfonso-Prieto, M.; Biarnes, X.; Vidossich, P.; Rovira, C. The Molecular Mechanism of the Catalase Reaction. *J. Am. Chem. Soc.* **2009**, *131*, 11751−11761.
(61) Alfonso-Prieto, M.; Vidossich, P.; Rovira, C. The Reaction Mechanisms of Heme Catalases: An Atomistic View by *ab initio* Molecular Dynamics. *Arch. Biochem. Biophys.* **2012**, *525*, 121−130.
(62) Martí, M. A.; Crespo, A.; Bari, S. E.; Doctorovich, F. A.; Estrin, D. A. QM-MM Study of Nitrite Reduction by Nitrite Reductase of *Pseudomonas aeruginosa*. *J. Phys. Chem. B* **2004**, *108* (46), 18073−18080.
(63) Esquerra, R. M.; Jensen, R. A.; Bhaskaran, S.; Pillsbury, M. L.; Mendoza, J. L.; Lintner, B. W.; Kliger, D. S.; Goldbeck, R. A. The pH Dependence of Heme Pocket Hydration and Ligand Rebinding Kinetics in Photodissociated Carbonmonoxymyoglobin. *J. Biol. Chem.* **2008**, *283* (20), 14165−14175.

DOI: 10.1021/jp5093948
J. Phys. Chem. B 2015, 119, 1802−1813